Molecular Microbiology (2008) 69(1), 94–109 ■
doi:10.1111/j.1365-2958.2008.06260.x
First published online 7 May 2008

Ancestral roles of eukaryotic frataxin: mitochondrial frataxin function and heterologous expression of hydrogenosomal *Trichomonas* homologues in trypanosomes

Shaojun Long,[1] Milan Jirků,[1] Jan Mach,[2] Michael L. Ginger,[3†] Robert Sutak,[4] Des Richardson,[4] Jan Tachezy[2] and Julius Lukeš[1*]

[1]*Biology Centre, Institute of Parasitology, Czech Academy of Sciences, and Faculty of Natural Sciences, University of South Bohemia, České Budějovice (Budweis), Czech Republic.*

[2]*Faculty of Sciences, Charles University, Prague, Czech Republic.*

[3]*Sir William Dunn School of Pathology, University of Oxford, Oxford, UK.*

[4]*Department of Pathology and Bosch Institute, University of Sydney, Sydney, NSW, Australia.*

Summary

Frataxin is a small conserved mitochondrial protein; in humans, mutations affecting frataxin expression or function result in Friedreich's ataxia. Much of the current understanding of frataxin function comes from informative studies with yeast models, but considerable debates remain with regard to the primary functions of this ubiquitous protein. We exploit the tractable reverse genetics of *Trypanosoma brucei* in order to specifically consider the importance of frataxin in an early branching lineage. Using inducible RNAi, we show that frataxin is essential in *T. brucei* and that its loss results in reduced activity of the marker Fe–S cluster-containing enzyme aconitase in both the mitochondrion and cytosol. Activities of mitochondrial succinate dehydrogenase and fumarase also decreased, but the concentration of reactive oxygen species increased. Trypanosomes lacking frataxin also exhibited a low mitochondrial membrane potential and reduced oxygen consumption. Crucially, however, iron did not accumulate in frataxin-depleted mitochondria, and as *T. brucei* frataxin does not form large complexes, it suggests that it plays no role in iron storage. Interestingly, RNAi phenotypes were ameliorated by expression of frataxin homologues from hydrogenosomes of another divergent protist *Trichomonas vaginalis*. Collectively, the data suggest trypanosome frataxin functions primarily only in Fe–S cluster biogenesis and protection from reactive oxygen species.

Introduction

Frataxin homologues are widely distributed among both prokaryotes and eukaryotes (Lill and Mühlenhoff, 2006; Bedekovics *et al*., 2007), but despite many independent studies during the last 10 years, there are still uncertainties with regard to the exact physiological function of this protein family. Eukaryotic frataxin is a mitochondrial matrix-targeted protein (Bulteau *et al*., 2004; Stehling *et al*., 2004; Bencze *et al*., 2006). In humans, mutations that affect the expression or function of the frataxin gene (most commonly arising from a triplet-repeat expansion within intron 1) are responsible for the onset of Friedreich's ataxia, an autosomal recessive syndrome affecting 1 in 30 000–50 000 individuals (Bencze *et al*., 2006). At the cellular level, patients exhibit defective mitochondrial metabolism including increased mitochondrial iron content and loss of mitochondrial DNA.

Led by many informative studies using tractable yeast models, various biochemical and genetic studies have revealed monomeric frataxin (encoded in *Saccharomyces cerevisiae* by *yfh1*) binds iron and delivers it to IscU scaffoled proteins for the essential process of Fe–S cluster assembly (Mühlenhoff *et al*., 2002; Gerber *et al*., 2003; 2004; Yoon and Cowan, 2003; Ramazzotti *et al*., 2004; Stehling *et al*., 2004; Zhang *et al*., 2006; Martelli *et al*., 2007; Shan *et al*., 2007). A role for frataxin in iron delivery during haem biosynthesis also seems likely due to its interaction with ferrochelatase, which catalyses the last step in haem biosynthesis (Lesuisse *et al*., 2003; Park *et al*., 2003; Yoon and Cowan, 2004; Cook *et al*., 2006). There remains some considerable debate, however, as to the extent of frataxin's primary functions. Thus, numerous studies with various animal and yeast models have failed

Accepted 11 April, 2008. *For correspondence. E-mail jula@paru.cas.cz; Tel. (+420) 38 7775416; Fax (+420) 38 5310388. †Present address: Department of Biological Sciences, Lancaster University, Lancaster, UK.

to reveal unequivocally whether different phenotypes often seen in frataxin mutants (e.g. mitochondrial iron accumulation, increased sensitivity to reactive oxygen species (ROS), impaired haem synthesis) arise as a consequence of secondary defects due to the failure of Fe–S cluster assembly, or if frataxin actually functions more generally as a protein required for intracellular, or more specifically intramitochondrial, control of iron homeostasis (Cavadini *et al*., 2000; Foury and Talibi, 2001; Lesuisse *et al*., 2003; Campanella *et al*., 2004; Santos *et al*., 2004; Gonzalez-Cabo *et al*., 2005; Schoenfeld *et al*., 2005). Some of the experimental observations that give rise to the uncertainties regarding frataxin function have been recently summarized (Irazusta *et al*., 2006).

One possibility to gain further insight into frataxin function, and to address whether species-specific adaptations may have arisen during evolution is to study the functional role of the bacterial frataxin homologue CyaY (Bedekovics *et al*., 2007; Ding *et al*., 2007). However, bacteria often operate multiple functionally distinct systems for Fe–S cluster assembly, and some component proteins even appear to be required only for the maturation of dedicated targets (Takahashi and Tokumoto, 2002; Nachin *et al*., 2003; Johnson *et al*., 2005; Loiseau *et al*., 2007). Single-gene deletions of *CyaY* in *Escherichia coli* and *Salmonella enterica* show no obvious phenotype or perturbation to Fe–S cluster assembly (Li *et al*., 1999; Vivas *et al*., 2006), and while multiple deletions of *CyaY* and other genes implicated in Fe-handling do result in defective Fe–S cluster assembly and sensitivity to oxidative stress (Vivas *et al*., 2006), this still does not inform conclusively on frataxin function.

Another issue relating to the functional analysis of frataxin is that in the context of the eukaryotic tree of life, the evolutionary distances that separate yeast from animals are relatively small (Keeling *et al*., 2005). One possibility is that the acquisition of new frataxin functions occurred following the divergence of animals and fungi (collectively the 'opisthokonts') from other eukaryotes (e.g. the lineages that lead to land plants and many protists). Moreover, no frataxin homologue is annotated in the genome sequences of several *Plasmodium* species (van Dooren *et al*., 2006) or *Giardia lamblia* (Morrison *et al*., 2007). As the Fe–S cluster assembly process in these parasitic protozoa appears to be similar to *S. cerevisiae* (Tovar *et al*., 2003; van Dooren *et al*., 2006), current genome annotations suggest natural instances in evolution, where frataxin functions either are dispensable or can be assumed by other proteins.

Based on mitochondrial genome sequence, the most ancestral mitochondria – i.e. potentially closest in form and function to the proto-mitochondrion – are found in *Reclinomonas americana* (Lang *et al*., 1997), which belongs to the protist supergroup Excavata (Hampl *et al*., 2005; Keeling *et al*., 2005; Simpson *et al*., 2005; Rodríguez-Ezpeleta *et al*., 2007). This collection of flagellate protists also includes medically relevant parasites such as trypanosomes, *Leishmania*, *Trichomonas vaginalis* and *G. lamblia*. In addition to available mitochondrial genome sequences, other features of the cell biology associated with these protozoa (Morrison *et al*., 2007) suggest that collectively they plausibly represent the earliest diverging extant eukaryotes. Thus, we hypothesized that an analysis of frataxin function in the most experimentally tractable excavate, *Trypanosoma brucei* (causative agent of African sleeping sickness), would provide an indication of the ancestral function of frataxin during eukaryotic evolution. Here we report the results of that investigation.

Results

Identification of T. brucei *frataxin*

In the *T. brucei* genome a single-copy gene with a significant sequence similarity to eukaryotic frataxin (Tb-frataxin) was identified. The Tb-frataxin coding region is 540 nt long with a predicted molecular mass of 19.4 kDa. The protein contains a cleavable mitochondrial import signal, predicted by PsortII, TargetP and Mitoprot to be 47 amino acids long in *T. brucei* (Fig. 1, underlined). The amino acid alignment with frataxins from other organisms revealed an overall low similarity, especially in the N-terminal half of the gene. The overall similarity between Tb-frataxin and frataxins from yeast and human is 35% and 48% respectively: the central region of frataxin contains a few conserved residues and the most significant conservation is confined to the C-terminal region of the protein (Fig. 1). Importantly, the characteristic frataxin topology, as derived from crystal structures of yeast, human and bacterial orthologues (six β-sheets and two α-helices), is conserved in *T. brucei*. Out of 9 and 30 residues implicated in iron and ferrochelatase binding, respectively, in yeast and human frataxin, 8 and 19 residues are conserved in Tb-frataxin (Fig. 1, asterisks and hash marks).

Phylogenetic analysis by maximum likelihood based on the amino acid sequences of a number of prokaryotic and eukaryotic frataxin genes suggests *T. brucei* constitutes an early branching eukaryotic lineage and that all available frataxins from kinetoplastids (*Trypanosoma* and *Leishmania* species) are closely related (Fig. 2). Although mutual relationships among the eukaryotic clades are not resolved due to low information content in the frataxin sequences, the origin of all eukaryotic frataxins from α-proteobacteria is strongly supported by bootstrap values (Fig. 2).

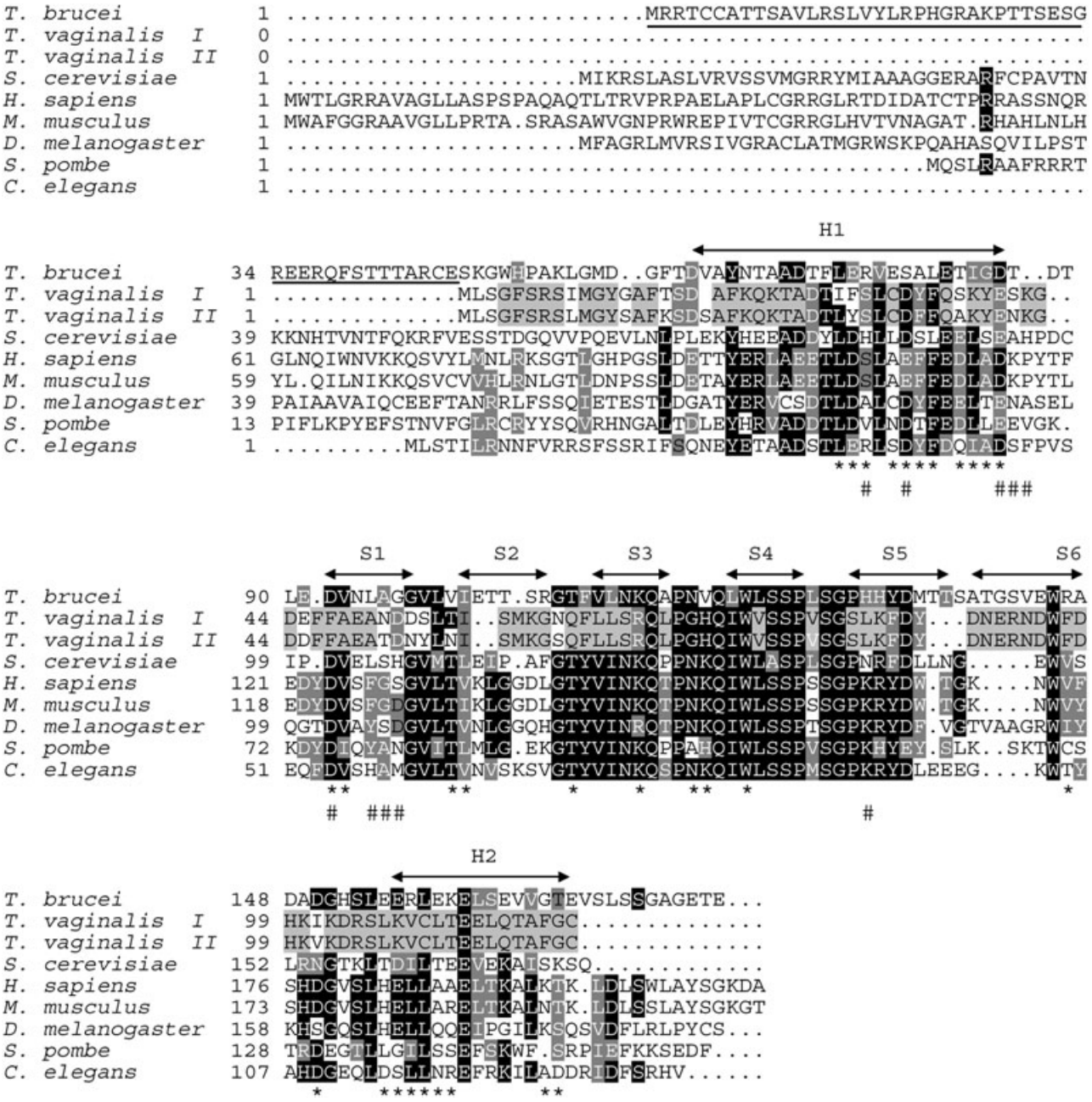

Fig. 1. Multiple alignment of predicted protein sequences of frataxin from *Trypanosoma brucei*, *Trichomonas vaginalis* (I and II), *Saccharomyces cerevisiae*, *Homo sapiens*, *Mus musculus*, *Drosophila melanogaster*, *Schizosaccharomyces pombe* and *Caenorhabditis elegans*. Amino acids are numbered to the left of the respective sequences. Conserved positions are in black, conservatively substituted in grey, and variable positions in white. Gaps were introduced to optimize the alignment. The mitochondrial targeting sequence of *T. brucei* frataxin is underlined. Asterisks and hash marks denote residues implicated in iron and ferrochelatase binding. The position of α-helices (H1 and H2) and β-sheets (S1–S6) are indicated above the alignment.

Localization and sedimentation properties of Tb-frataxin

The life cycle of *T. brucei* is complex and involves transmission cycles in both a mammalian host and a tsetse fly vector. Both procyclic (tsetse midgut form) and pathogenic bloodstream trypanosomes can be grown in liquid culture. To verify its predicted mitochondrial localization, Tb-frataxin was expressed in *E. coli*, and polyclonal antibodies were raised against purified recombinant protein. Initially, procyclic trypanosomes were fractionated by extraction with increasing concentrations of digitonin; Tb-frataxin was detected by immunoblot analysis in the mitochondria-rich fraction, whereas no signal was observed in the cytosol (Fig. 3A). Subsequent indirect

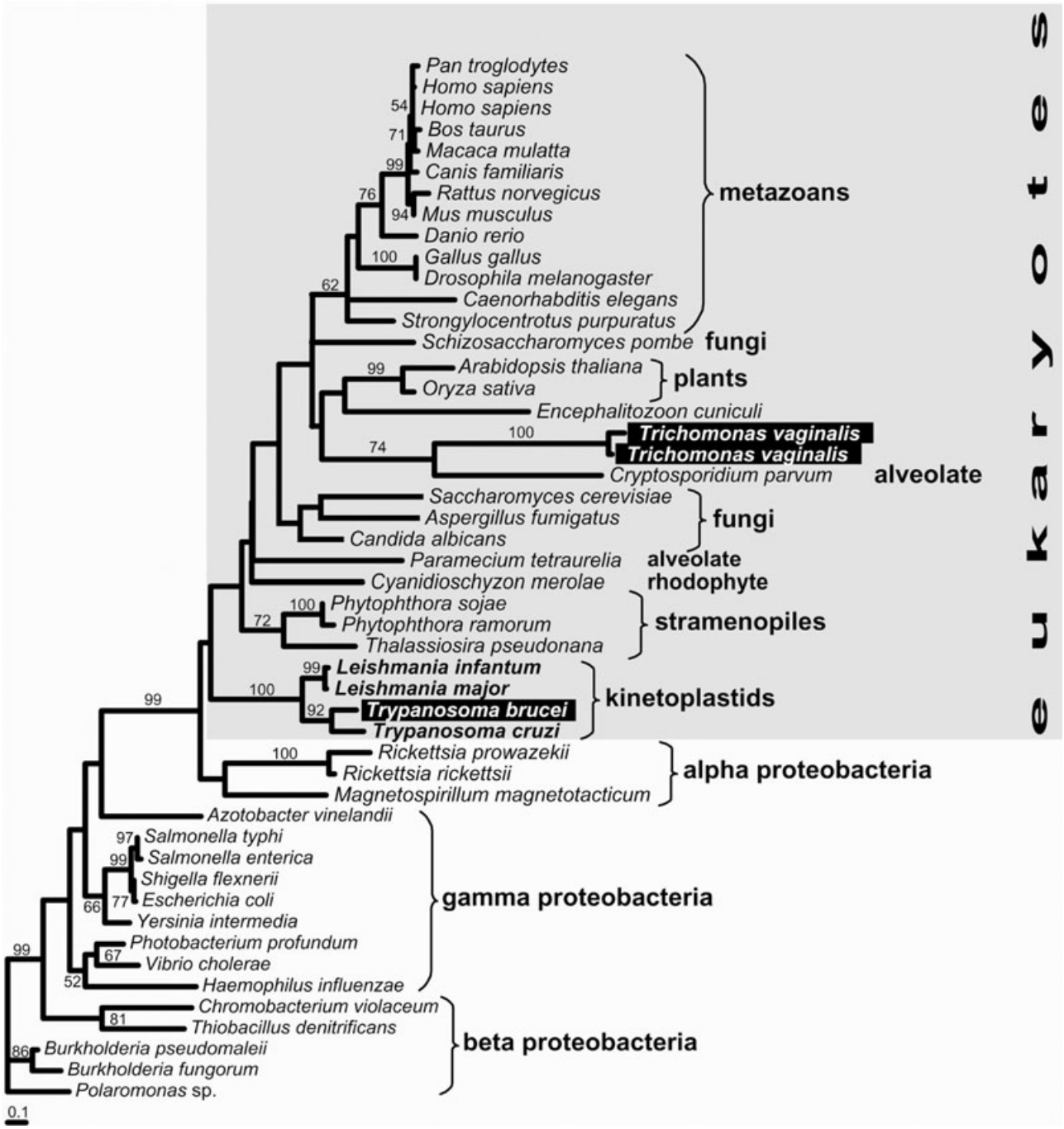

Fig. 2. Maximum-likelihood tree inferred from the amino acid sequences of frataxin in selected prokaryotes and eukaryotes (WAG matrice, γ distribution in four categories). Numbers above branches indicate bootstrap support for maximum parsimony (only values over 50% are shown).

immunofluorescence experiments revealed an even distribution of protein throughout the reticulated mitochondrion (Fig. 3B); mitochondrial localization was confirmed by co-immunolocalization of Tb-frataxin with mitotracker (Fig. 3B). Human, mouse and yeast frataxins are known to exist as stable monomers and/or form large oligomeric structures (Bencze *et al*., 2006; Cook *et al*., 2006). To test in which form Tb-frataxin is present *in vivo*, total lysates from procyclic and bloodstream cells were analysed by glycerol gradient sedimentation. Probing the gradient fractions with α-Tb-frataxin antibodies revealed that in both stages Tb-frataxin sediments in the six uppermost

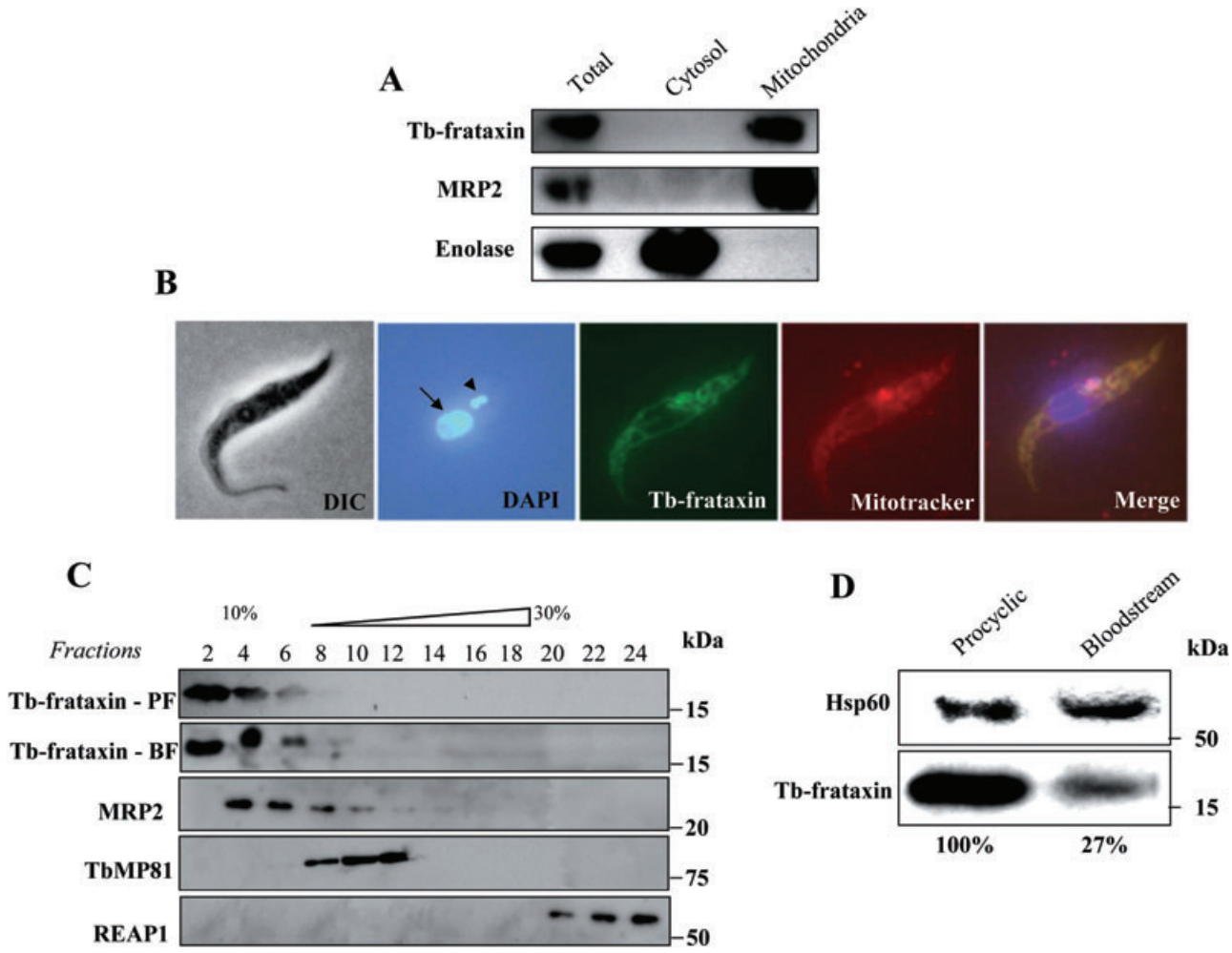

Fig. 3. Expression and localization of frataxin in *T. brucei*.
A. Immunoblot analysis of Tb-frataxin expression in whole-cell lysates and purified cytosolic and mitochondrial fractions of procyclic *T. brucei*. MRP2 and enolase proteins were used as mitochondrial and cytosolic marker proteins respectively.
B. Immunolocalization of Tb-frataxin shows an even distribution in the reticulated mitochondrion of procyclic *T. brucei*. Mitotracker Red staining, 4′,6-diamidino-2-phenylindole staining (DAPI) and immunolocalization of Tb-frataxin. Arrowhead and arrow indicate kinetoplast and nuclear DNA respectively. The merged image is given for colocalization of Tb-frataxin with mitotracker. DIC, differential interference contrast.
C. Sedimentation analysis of Tb-frataxin. Cleared lysates of mitochondria isolated hypotonically from procyclic and bloodstream-form parasites mitochondria were loaded onto glycerol gradients and fractionated as described elsewhere (Vondrušková *et al*., 2005). Fractions from each gradient were analysed by SDS-PAGE and immunoblotted with α-Tb-frataxin, α-MRP2, α-TbMP81 and α-REAP1 antibodies; the last three antibodies were used as sedimentation markers.
D. Immunoblot analysis of Tb-frataxin in procyclic and bloodstream trypanosomes. Whole-cell lysates from procyclic 29-13 (PF) and bloodstream 920 (BF) cells were immunoblotted with α-Tb-frataxin and α-Hsp60 antibodies. The latter antibody represents a loading control. Quantification of Tb-frataxin signal is also shown.

fractions, with the majority present in fraction 2, revealing that Tb-frataxin does not form large complexes in trypanosomes (Fig. 3C). The sedimentation profiles of several mitochondrial proteins involved in RNA editing [mitochondrial RNA-binding protein 2 (MRP2), editosomal protein TbMP81 and RNA editing-associated protein 1 (REAP1)] were in agreement with previously published results (Vondrušková *et al*., 2005) and validated the gradients. Probing cell lysates from procyclic and bloodstream *T. brucei* revealed frataxin is much less abundant in the latter form (Fig. 3D), in which the mitochondrion does not participate directly in ATP production and a typical mitochondrial respiratory chain is absent.

Effect of RNAi against Tb-frataxin

In order to study Tb-frataxin function, we stably transfected a procyclic 29-13 cell line with a p2T7-177 RNAi vector (Wickstead *et al*., 2002) bearing a fragment of the Tb-frataxin gene. For experiments described here, a clonal cell line was selected that responded to tetracycline-inducible RNAi by almost complete elimina-

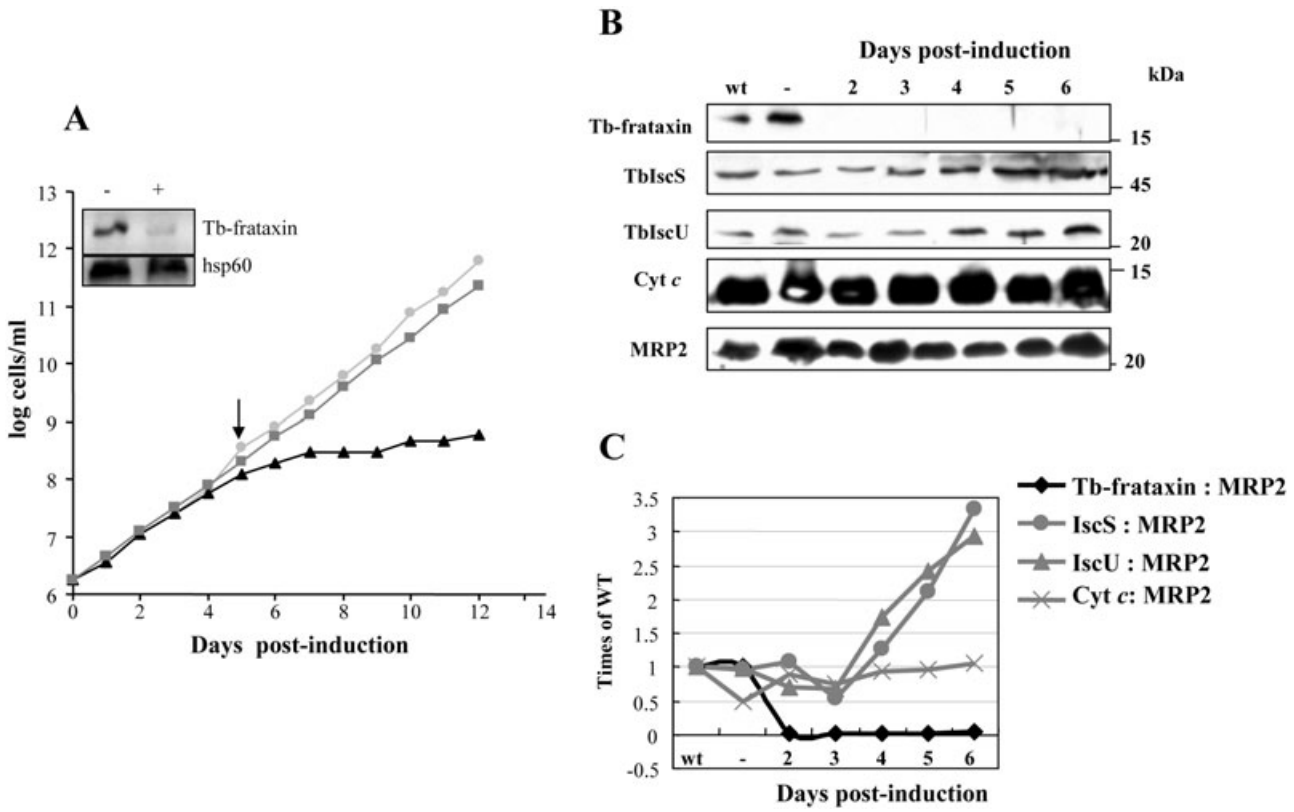

Fig. 4. Effect of Tb-frataxin RNAi on parasite growth and the expression of mitochondrial proteins.
A. Cell densities were measured using Beckman Z2 Coulter. The numbers of the parental 29-13 cell line (dots), RNAi non-induced (squares) and RNAi-induced cells (triangles) are indicated. The *y*-axis is labelled by a log scale and represents the products of measured cell densities and the total dilution. The arrow represents sampling site for latter experiments.
B. Expression levels of frataxin, cysteine desulphurase (TbIscS2), metallochaperone (TbIscU), cytochrome *c* (Cyt *c*) and mitochondrial RNA-binding protein 2 (MRP2) as determined by immunoblot analysis of whole-cell lysates of the parental 29-13 cell line (wt), and the RNAi knock-down cells both before (–) and after 2–6 days of RNAi induction. MRP2 represents a loading control in these experiments.
C. Quantification of the immunoblot analysis in (B) with Bio-Rad quantity one. The *y*-axis shows abundance of the followed proteins as compared with the wild-type levels.

tion of the target protein after 2 days of induction (Fig. 4B, top). The repression of Tb-frataxin expression by RNAi had no effect on the levels of assayed cytochrome *c*, whereas cysteine desulphurase (TbIscS) and metallochaperone (TbIscU), two other proteins involved in the Fe–S cluster assembly in the *T. brucei* mitochondrion (Smíd *et al.*, 2006), were somewhat upregulated by day 4 of RNAi induction (Fig. 4B and C). The growth rate of RNAi-induced cells slowed by day 4 of induction and then ceased completely by day 6 (Fig. 4A). The morphology of induced cells after they stopped dividing appeared normal by both light and electron microscopy, and even after 1 week of induction no alteration of the kinetoplast DNA was observed, as judged by DAPI staining (data not shown).

To test whether elimination of Tb-frataxin resulted in a decrease or disruption of Fe–S cluster assembly, we measured the activities of marker Fe–S cluster-containing enzymes aconitase, fumarase and succinate dehydrogenase. The dual localization of the *T. brucei* aconitase [30% of measurable activity is cytosolic and 70% is mitochondrial (Saas *et al.*, 2000)] allowed us to determine whether Tb-frataxin is needed for Fe–S cluster incorporation into the mitochondrial and/or cytosolic pools of aconitase. Upon RNAi induction, a dramatic overall decrease of aconitase activity was observed after only 2 days of induction, with the decrease in the cytosolic compartment being much more pronounced (Fig. 5A). Western blot analysis of total cell, cytosolic and mitochondrial lysates revealed that the drop in aconitase activity was not caused by lower expression or degradation of the protein (Fig. 5B), but most likely by the impairment or absence of the enzyme's [4Fe–4S] cluster. A similar dramatic decrease in enzyme activity was observed for another Fe–S cluster-containing enzyme, fumarase (Fig. 5C), but in contrast the activity of threonine dehydrogenase, an enzyme without Fe–S clusters, remained unaltered following RNAi induction (Fig. 5E).

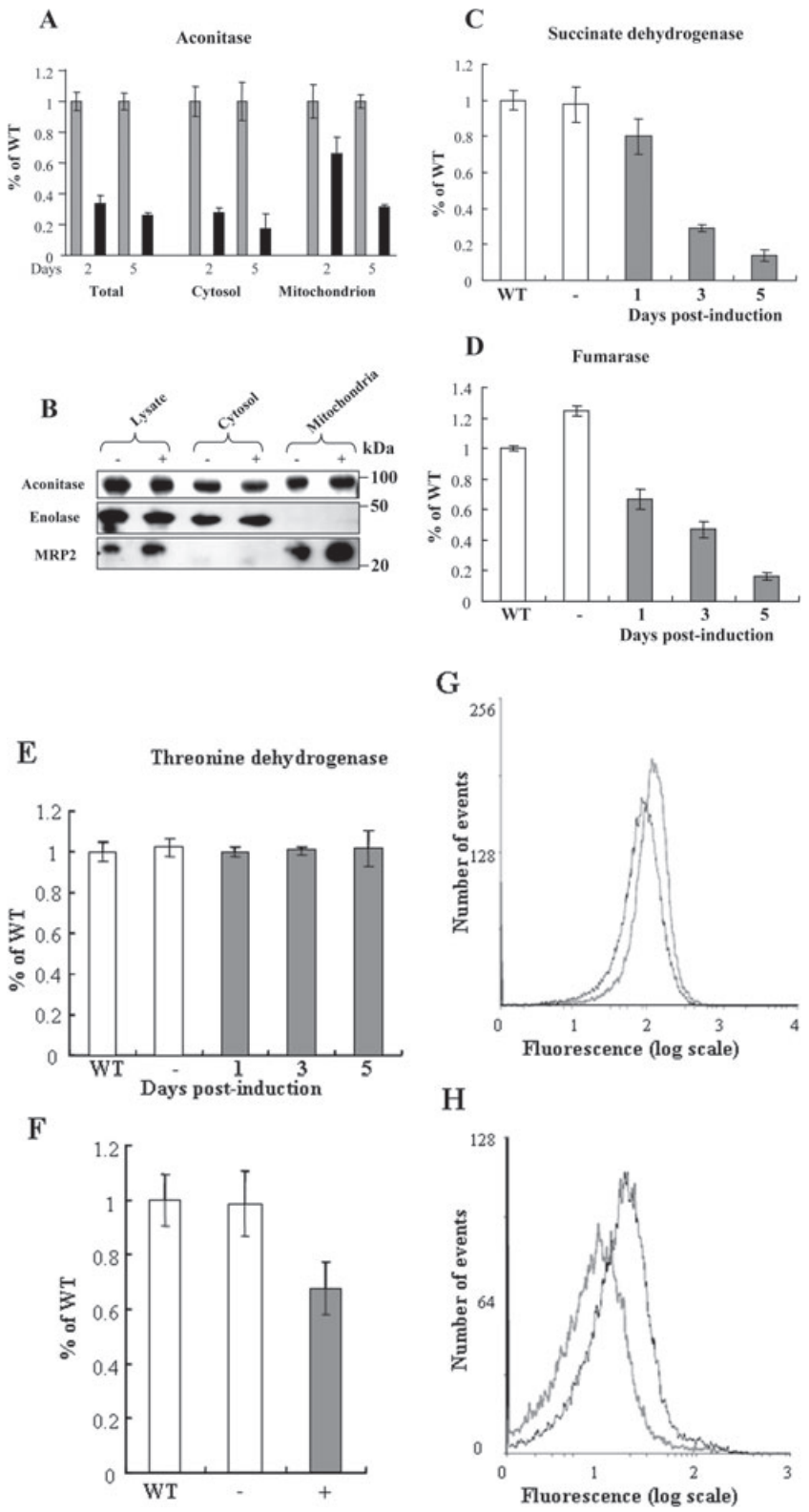

Fig. 5. Metabolic consequences of inducing Tb-frataxin RNAi. The effects of Tb-frataxin RNAi on the activity (A) and abundance (B) of the Fe–S cluster-containing enzyme aconitase, and the activities of two other Fe–S cluster-containing enzymes succinate dehydrogenase (C) and fumarase (D), threonine dehydrogenase, which does not possess a Fe–S cluster cofactor (E), oxygen consumption (F), mitochondrial inner membrane potential (G) and reactive oxygen species accumulation (H) are all shown.
A. Percentage of specific activities of aconitase in total-cell lysate, cytosol and mitochondria in cells before (grey columns), and after 2 and 5 days of RNAi induction (black columns) is shown. The mean and the SD values represent the averages of three experiments.
B. The amount of aconitase present in the total-cell lysate plus cytosolic, and mitochondrial fractions is shown. Cells were fractionated by extraction with digitionin before (–) and after (+) 5 days of RNAi induction and used for immunoblot analysis with α-aconitase, α-enolase (cytosolic marker) and α-MRP2 antibodies (mitochondrial marker).
C–E. The activities of succinate dehydrogenase (complex II), fumarase and threonine dehydrogenase were measured in total-cell lysates of parental (WT) and RNAi cell lines, before (–) and after 1, 3 and 5 days of RNAi induction.
F. Measurement of O_2 consumption. Wild-type (empty column) and non-induced cells (empty column), and cells 5 days after RNAi induction (grey column) were incubated in SDM-79 medium at 27°C and O_2 consumption was monitored with a Clark electrode. The SD values of five independent RNAi inductions are shown.
G. Measurement of mitochondrial inner membrane potential. Membrane potentials were measured by flow cytometry in non-induced cells (grey line) and in cells 5 days after RNAi induction (black line) following incubation with 0.4% tetramethylrodamine ethyl ester (TMRE) for 20 min. Fluorescence distributions were plotted as frequency histograms. One representative experiment out of three performed is shown here.
H. Measurement of ROS accumulation. Non-induced cells (grey line) and cells after 5 days of RNAi induction (black line) were incubated in the presence of 5 μg ml^{-1} dihydroethidium for 30 min and analysed by flow cytometry. Representative data from four independent experiments are shown.

The presence and significance of a classical complex I (NADH dehydrogenase) activity in *T. brucei* is debatable. We therefore measured the activity of complex II (succinate dehydrogenase) as a proxy for respiratory chain activity. As expected for a Fe–S cluster-containing enzyme, its activity dropped to 10% of value in the wild-type cells (Fig. 5C). Procyclic trypanosomes are characterized by the presence of a branched mitochondrial electron-transport chain, comprising a classic cytochrome-dependent mitochondrial respiratory chain and alternative oxidase (Besteiro *et al*., 2005). As cytochrome-mediated respiration is dependent on the presence of Fe–S cluster-containing proteins and represents the dominant branch of the procyclic mitochondrial electron-transport chain, we anticipated a decrease in oxygen consumption in RNAi-induced cells. Indeed, a statistically significant decrease was observed (Fig. 5F). As mitochondrial inner membrane potential, at least in procyclic trypanosomes, generally requires adequate functioning of the individual respiratory complexes, we anticipated a decline in mitochondrial membrane potential, too. As quantified by the uptake of tetramethylrodamine ethyl ester (TMRE) and the use of flow cytometry, mitochondrial inner membrane potential also decreased substantially (Fig. 5G). We also measured the accumulation of ROS in both non-induced and induced cells using the reagent dihydroethidium. A significant difference between the non-induced and induced cells was observed, indicating that cells lacking Tb-frataxin accumulate more ROS (Fig. 5H). In terms of changes to metabolic flux as a result of the impact of RNAi on the activities of various mitochondrial enzymes, we observed a considerable increase in the abundance of pyruvate as an end-product (Fig. 6A). Other measured metabolic end-products (succinate, malate, fumarate and acetate) did not show any significant changes (data not shown). We previously reported a similar shift in metabolic end-product excretion following RNAi against either TbIscS or TbIscU (Smíd *et al*., 2006). As accumulation of free iron is a classic hallmark consequence of the decrease or dysfunction of frataxin in the human cells and yeast mutants, we measured total cellular and mitochondrial iron concentration following induction of Tb-frataxin RNAi. Unexpectedly, even after several days of induction, iron did not accumulate in the organelle. In fact, the concentration of iron in four independent inductions was even somewhat lower in the knock-down cells (~80% of the wild-type level, which was 187 ± 28 μg per gram of protein). In contrast, the concentration of zinc remained unaffected following RNAi induction (Fig. 6B).

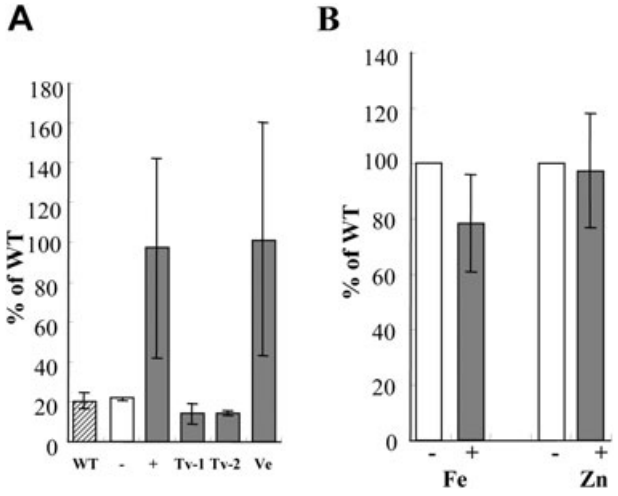

Fig. 6. Metabolic consequences of inducing Tb-frataxin RNAi II. The effect of Tb-frataxin RNAi on end-products of glucose metabolism and Fe and Zn content.
A. Effect of Tb-frataxin RNAi on end-products of glucose metabolism. The graph shows relative concentration of end-products as detected by HPLC for parental 29-13 cells (WT; stripped column) and cells before (–; empty column) and after 5 days of RNAi induction (+; grey columns). Tv-1 and Tv-2 represent RNAi-induced cells that constitutively expressed either of the two *Trichomonas* frataxins; Ve denotes RNAi-induced cells that contained an empty pABPURO vector. Mean and the SD values from four independent experiments are shown.
B. ICP-AES estimation of iron (Fe) and zinc (Zn) content in the mitochondria of RNAi non-induced cells (empty columns) and in cells after 5 days of RNAi induction (grey columns). The mean and the SD values of four independent experiments are shown.

Rescue of RNAi phenotypes by hydrogenosomal T. vaginalis *frataxins*

Recently, a frataxin from the hydrogenosomes of *T. vaginalis* (Tv-frataxin) was shown to partially restore defects in haem and Fe–S cluster synthesis in *yfh1*-deficient *S. cerevisiae* (Dolezal *et al*., 2007). Yet, in the genome of *T. vaginalis* two closely related frataxin genes are present (Carlton *et al*., 2007). These isoforms possibly arose as a consequence of whole genome duplication, rather than merely a single gene duplication event, but *T. vaginalis* represents the only known example of an organism with two frataxin homologues (Tv-frataxin-1 and Tv-frataxin-2). As *T. vaginalis* is relatively intractable with regard to functional genomics, we decided to functionally assay both Tv-frataxins in *T. brucei*. Full-length Tv-frataxin-1 and -2 genes (i.e. encoding proteins with a hydrogenosomal targeting sequence) were cloned into the pABPURO vector, which following stable integration into the trypanosome genome facilitates constitutive expression of the inserted gene (Rusconi *et al*., 2005).

The pABPURO constructs containing either Tv-frataxin-1 or Tv-frataxin-2 were integrated into the nuclear genome of the Tb-frataxin RNAi cell line used in the experiments described above (Figs 3–5). As a control,

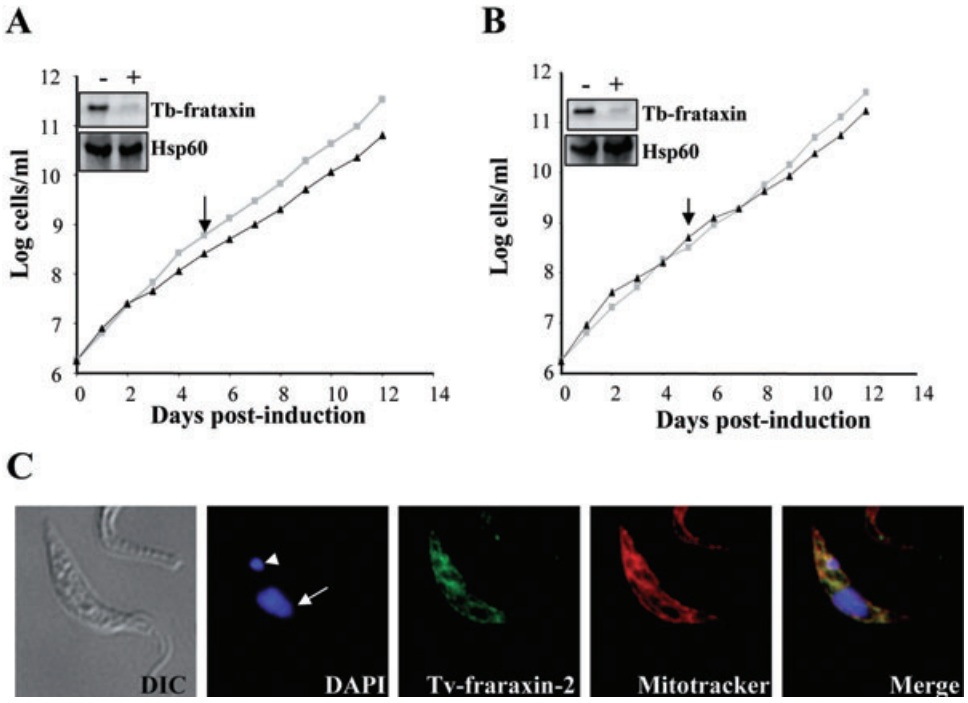

Fig. 7. Effect of the introduction of *T. vaginalis* frataxins into *T. brucei* (Tb) frataxin RNAi cells and immunolocalization of Tv-frataxin-2. Representative data from four independent experiments are shown.
A and B. Effect of the introduction of Tv-frataxin-1 (A) and Tv-frataxin-2 (B) on the growth of non-induced cells (grey line) and cells interfered against Tb-frataxin (black line). The insets show Western blots of the total lysate from cells before (–) and after 5 days of RNAi induction (+) immunoblotted with the α-Tb-frataxin (top) and α-hsp60 (bottom; loading control) antibodies. The growth curves were performed as in Fig. 4B. The vertical arrows indicate the date of sampling.
C. Immunostaining of procyclic *T. brucei* expressing HA3-tagged Tv-frataxin-2 shows its even distribution in the reticulated mitochondrion. Mitotracker Red staining (MTR), 4′,6-diamidino-2-phenylindole staining (DAPI) and immunolocalization of Tv-frataxin-2. Arrowhead and arrow indicate kinetoplast and nuclear DNA respectively. The merged image is given for colocalization of Tv-frataxin-2 with mitotracker. DIC, differential interference contrast.

pABPURO vector lacking a frataxin gene was also integrated into the RNAi cell line. Following the selection of three new RNAi cell lines with puromycin (one cell line expressing Tv-frataxin-1, one expressing Tv-frataxin-2, and one containing only the empty pABPURO vector), efficient RNAi-dependent downregulation of Tb-frataxin was still achieved by the addition of tetracycline, as judged from Western blot analysis with α-Tb-frataxin antibodies (Fig. 7A and B, insets). As no antibody that detects *T. vaginalis* frataxins is available, constitutive transcription of both trichomonad genes was confirmed by Northern blot analysis, with wild-type *T. brucei* and Tb-frataxin RNAi cells serving as negative controls (Fig. S1). We also stably expressed a fusion of Tv-frataxin-2 with a haemagglutinin (HA3)-tag attached to its C-terminus. As expression was mediated by a strong procyclin promoter, the concentration of fusion protein could have been higher than that of endogenous Tb-frataxin. In spite of a possible overexpression, however, we saw epitope-tagged Tv-frataxin-2 was distributed evenly throughout the mitochondrion, with no protein detected in the trypanosome cytosol (Fig. 7C).

Importantly, expression of neither Tv-frataxin-1 nor Tv-frataxin-2 affected the growth rate of procyclic cultures (Fig. 7A and B), when compared with either non-induced Tb-frataxin RNAi cells (Fig. 4B) or cells containing empty vector (data not shown). Moreover, following induction of Tb-frataxin RNAi, growth of non-induced and induced cells was similar for both the Tv-frataxin-1 and Tv-frataxin-2 expressing cell lines. In addition, mitochondrial membrane potential was retained where the RNAi background was complemented by expression of either *Trichomonas* frataxin (Fig. S2A and B), whereas Tb-frataxin RNAi cells transformed with empty pABPURO exhibited a reduced membrane potential upon induction (Fig. S2C). ROS measurements yielded an analogous complementation, with the amount of ROS produced in RNAi-induced cells remaining at almost wild-type levels following expression of the Tv-frataxin (Fig. S2D and E). Activities of several Fe–S cluster-containing enzymes were also measured, revealing that in the presence of trichomonad frataxins the activities of aconitase, succinate dehydrogenase and fumarase in cells induced for RNAi against Tb-frataxin were all significantly higher than

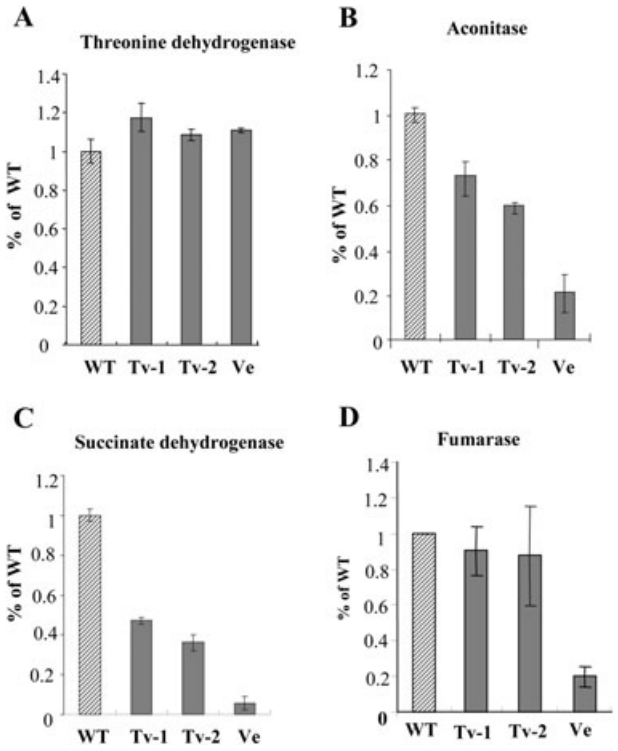

Fig. 8. Activities of selected enzymes containing or lacking Fe–S cluster(s) were measured in total lysates of Tb-frataxin RNAi cells after 5 days of induction, induced Tb-frataxin RNAi cells transformed with either pABPURO containing Tv-frataxin-1 (Tv-1), Tv-frataxin-2 (Tv-2) or an empty pABPURO vector (Ve). Activities in wild type are shown in stripped columns, activities in Tb-frataxin RNAi cells transformed with Tv-frataxin-1 and -2, and with an empty pABPURO vector are shown in grey columns. The mean and the SD values of five experiments are shown.
A. The activities of threonine dehydrogenase, a non-Fe–S cluster protein.
B–D. The activities of Fe–S cluster-containing aconitase (B), succinate dehydrogenase (complex II) (C) and fumarase (D).

in RNAi-induced cells which contained only the empty pABPURO vector (Fig. 8) or in the original Tb-frataxin RNAi cell line (Fig. 5). In the example of fumarase, the enzyme activity observed in Tv-frataxin-1 and Tv-frataxin-2 expressing cells was at near wild-type levels (Fig. 8D). Collectively, these data indicate efficient complementation of the Tb-frataxin RNAi phenotype following heterologous expression of *Trichomonas* frataxins.

Discussion

The trypanosome model for studying frataxin function

Despite its small size and a lack of well-defined domains, frataxin has been implicated in tractable yeast and mammalian experimental systems with a variety of functions associated with iron metabolism, including Fe–S cluster assembly, haem biosynthesis, iron storage, respiratory regulation and oxidative stress protection (Foury *et al.*, 2001; Muhlenhoff *et al.*, 2002; Gerber *et al.*, 2003; Lesuisse *et al.*, 2003; Yoon and Cowan, 2003; Bulteau *et al.*, 2004; Ramazzotti *et al.*, 2004; Santos *et al.*, 2004; Stehling *et al.*, 2004; Gonzáles-Cabo *et al.*, 2005; Schoenfeld *et al.*, 2005; Gakh *et al.*, 2006; Martelli *et al.*, 2007; Shan *et al.*, 2007). Yet the precise function of this ubiquitous protein remains uncertain. As most of the available knowledge about frataxin function pertains only to studies with yeast and animal cells, we hypothesized that a functional analysis of frataxin in a deep-branching excavate protozoan would be informative.

In some excavates (e.g. *Trichomonas*, *Giardia*) mitochondrial function has been streamlined through loss of a classical electron-transport chain and the capacity for oxidative phosphorylation (Embley, 2006). Although *Trichomonas* hydrogenosomes and *Giardia* mitosomes function in Fe–S cluster biogenesis, the loss of many classic mitochondrial pathways suggests trichomonads and diplomonads are not likely to present ideal experimental systems to study the core functions of frataxin. In contrast, the human pathogen *T. brucei* is an obligate aerobe and in its insect procyclic form possesses a mitochondrial respiratory chain. In pathogenic blood-form trypanosomes, however, the mitochondrion does not function directly in energy generation: here glycolysis is the sole ATP-generating pathway, and electrons are transferred from NADH to ubiquinone via mitochondrial glycerol-3-phosphate dehydrogenase, and from ubiquinol to oxygen by the constitutively expressed alternative oxidase (Besteiro *et al.*, 2005). Thus, African trypanosomes provide a good excavate model to study frataxin function, and interestingly one in which function can be studied under circumstances where the demand for iron or Fe–S clusters is naturally either high or low.

Nuances of frataxin function and the Tb-frataxin RNAi phenotype

The analyses by subcellular fractionation and immunofluoresence strongly indicate that in *T. brucei* frataxin is exclusively a mitochondrial protein, and that its expression levels correlate with intracellular iron demand in the two life cycle stages which can be propagated in culture. Human and yeast frataxins form stable monomers when operating as iron chaperone (Bencze *et al.*, 2006; Cook *et al.*, 2006), but bacterial, mouse and human frataxins can all oligomerize into large ~1 MDa assemblies that store iron (Cavadini *et al.*, 2000; O'Neill *et al.*, 2004). Crucially, glycerol gradient sedimentation assays in both procyclic and bloodstream forms revealed no evidence for oligomerization of *T. brucei* frataxin *in vivo*, suggesting that the protein plays no role in iron storage. Similarly, although loss of numerous Fe–S cluster-containing enzymes and an alteration of metabolic flux were evident in the induced Tb-frataxin RNAi

mutant (see below), no intracellular accumulation of iron occurred. Indeed, an absence of potentially destructive Fenton chemistry as a result of iron accumulation was further evidenced by a lack of discernible change to the appearance of the DAPI-stained kinetoplast DNA. The deeply divergent evolutionary status for the Excavata supergroup, downregulation of frataxin expression in response to increased extracellular iron availability in another excavate *T. vaginalis* (Dolezal *et al*., 2007), and the data presented here all support a hypothesis postulating that any role for frataxin with regard to general intramitochondrial iron distribution in animals and yeast is likely to be a derived rather than ancestral state. One could argue that adaptation to a parasitic lifestyle and the specific niche environment of the tsetse fly digestive tract has influenced the manner in which *T. brucei* acquires, stores and utilizes iron. However, the semi-defined SDM-79 medium used to culture procyclic trypanosomes provides an iron-replete medium, and the lack of mitochondrial iron accumulation provides a convincing indication that neither Tb-frataxin nor the mitochondrion plays any role in iron storage or that perturbation to the process of Fe–S cluster assembly leads to increased iron flux in trypanosomes. Results from an elemental analysis of the American trypanosome species *Trypanosoma cruzi* using ultracryomicrotomy and electron probe microanalysis previously provided a quantitative analysis of iron distribution within epimastigotes, and suggested that trypanosomatids may, like yeast, accumulate iron within vacuolar reserves (Scott *et al*., 1997). Like *S. cerevisiae*, there is no indication that ferritin can be used to store iron.

In addition to reduced incorporation of Fe–S clusters into key target proteins and a lack of mitochondrial iron accumulation, another characteristic of the Tb-frataxin RNAi phenotype was an accumulation of ROS. Although we had anticipated that ROS accumulation, which is one of the hallmark characteristics of Friedreich's ataxia, would occur following downregulation of frataxin, the informative surprise was that this accumulation occurred in the absence of increased mitochondrial iron accumulation. This result therefore supports a recent prediction from Lesuisse and co-workers that ROS accumulation in yeast mutants lacking *yfh1* is not linked to an increase in mitochondrial iron polls (Bulteau *et al*., 2007). We do not know whether the primary cause of ROS accumulation in Tb-frataxin RNAi mutants was due to a change in respiratory rate. However, our data are also consistent with previous suggestions that an important primary function of frataxin is the limitation of ROS-induced damage (Gakh *et al*., 2006); further experiments will be necessary to determine whether in trypanosomes this protective role occurs via detoxification of inappropriate mitochondrial iron species or some other mechanism (e.g. direct or indirect regulation of respiratory rate).

As in other eukaryotes, mitochondrial Fe–S cluster assembly is essential in *T. brucei* (Smíd *et al*., 2006). The results presented here suggest that in this flagellate frataxin is also likely to be an essential gene; although oxidative phosphorylation appears not to be essential for procyclic trypanosomes grown in glucose-containing SDM-79 medium (Bochud-Allemann and Schneider, 2002; Besteiro *et al*., 2005), cytochrome-dependent respiratory chain activity is nonetheless essential for growth (Bochud-Allemann *et al*., 2002; Horváth *et al*., 2005). Moreover, carbohydrates are not considered to be a readily available carbon source within the digestive tract of a tsetse fly (Ginger, 2006), and in the absence of glucose procyclic cells are critically dependent on oxidative phosphorylation for viability (Besteiro *et al*., 2005). Thus, the reliance of *T. brucei* on respiratory chain activity and the likely importance of oxidative phosphorylation during the transmission cycle of trypanosomes through tsetse indicate frataxin is essential.

A potentially interesting aspect of the Tb-frataxin RNAi phenotype was increased loss of cytoplasmic aconitase activity, relative to mitochondrial aconitase activity. While this result may merely reflect differences in turnover time of the protein or the lability of the enzyme's Fe–S cluster in these two cellular compartments, this result could be interpreted as preliminary evidence that when the availability of Fe–S clusters is limiting, a hierarchical substrate preference of cytoplasmic Fe–S cluster handling CIA machinery becomes apparent. For instance, under such circumstances perhaps Fe–S clusters are preferentially inserted into key targets such as the highly conserved Rli1 protein (Kispal *et al*., 2005); growth of *T. brucei* has previously been shown to be critically dependent on Rli1 expression levels (Estévez *et al*., 2004). Finally, as trypanosomes are auxotrophic for haem and lack ferrochelatase, any direct role for frataxin in trypanosome haem metabolism appears very unlikely.

Frataxin – a universal component of the mitochondrial Fe–S cluster assembly apparatus

In Fe–S cluster assembly, frataxin is generally considered to act as an iron donor for the ISU1 scaffold. However, in glycerol-containing media frataxin-deficient *S. cerevisiae* maintains a high respiratory activity (Foury *et al*., 2001) and supplementation of YPD medium with additional manganese ameliorates the decline in activity of several Fe–S cluster-containing enzymes in yeast mutants lacking frataxin (Irazusta *et al*., 2006). On the other hand, one might suggest that these examples of frataxin-independent Fe–S cluster assembly are merely the result of manipulating laboratory growth media. On the other hand, the genome annotations of the excavate *G. lamblia* and several malarial parasites indicate there may be

natural examples of eukaryotes that use an ISC-style apparatus for Fe–S cluster assembly (Lill and Muhlenhoff, 2006), but which lack a frataxin orthologue. *Giardia* harbours unusual Fe–S cluster-containing targets, such as pyruvate:ferredoxin oxidoreductase, whereas *Plasmodium* species harbour a repertoire of mitochondrial and cytoplasmic Fe–S cluster-containing proteins that is similar to many other eukaryotes. The two yeast homologues, Isa1 and Isa2, of a bacterial iron delivery protein have also previously been considered to play pivotal roles in the delivery of iron for Fe–S cluster assembly (Jensen and Culotta, 2000; Kaut *et al*., 2000; Pelzer *et al*., 2000), but our results indicate that with respect to likely iron donors, predicted *T. brucei* orthologues of neither Isa1 nor Isa2 are able to compensate for the loss of frataxin in providing an adequate supply of iron for Fe–S cluster assembly.

Rescue of the Tb-frataxin RNAi phenotype by hydrogenosomal Tv-frataxins

Hydrogenosomal targeting signals from *T. vaginalis* have been shown to fetch a passenger protein into the *T. brucei* mitochondrion (Hausler *et al*., 1997). Here we have shown that the recognition and import of either of the two *T. vaginalis* frataxins via their endogenous hydrogenosomal import signals results in complementation of the Tb-frataxin RNAi phenotype. Even though the sequences of *Trichomonas* and *Trypanosoma* frataxins are very divergent, the rescue of the RNAi phenotype was extensive and included rescues of growth, mitochondrial inner membrane potential, various enzyme activities (to near wild-type levels in the case of fumarase) and a reduction in ROS levels to near wild-type levels. Interestingly, although expression of *Trichomonas* frataxin was able to rescue many of the phenotypes seen in *S. cerevisiae* Δ*yfh1* mutants, the yeast mitochondrial import machinery was unable to utilize the hydrogenosomal import signal, and heterologous rescue required fusion of trichomonad frataxin to a *bona fide* yeast mitochondrial import signal (Dolezal *et al*., 2007). While differences in evolutionary distance between yeast and trichomonads and trypanosomes and trichomonads might explain the ability of trypanosomes, but not yeast, to efficiently recognize the hydrogenosomal import signal for matrix target proteins, it should be interesting to look in comparative terms, and possibly even from the perspective of drug target characterization, at how the mitochondrial import machinery differs qualitatively between trypanosomes and other eukaryotes, including mammals. In that regard, the recent discussion regarding the probability of a simplified pathway for mitochondrial protein import in trypanosomes is relevant (Schneider *et al*., 2008). Overall and in summary, the results presented here further support the paradigm that the mitochondrion and, moreover, frataxin play fundamental, ancient and evolutionary conserved roles in cellular Fe–S cluster assembly.

Experimental procedures

Plasmid constructs, transfection, cloning and RNAi induction

The 5′ part of the *T. brucei* frataxin gene was PCR-amplified using oligonucleotides Tbftx1-F (5′-TTA*GGATCC*CTCAAAC TCACTTCAGTTCC-3′) and Tbftx1-R (5′-CCGAAGCTTA CCAGTGCAGTGCTACG-3′) (added BamHI and HindIII restriction sites are italicized and underlined respectively). The amplified fragment was cloned in the p2T7-177 vector, creating the construct Tb-frataxin-KD, which was subsequently electroporated into the procyclic *T. brucei* strain 29-13, and the clones were obtained as described elsewhere (Vondrušková *et al*., 2005). Synthesis of double-stranded RNA in stable RNAi transformants was induced by the addition of 1 μg ml^{-1} tetracycline to several clonal cell lines, obtained by limiting dilution in 96-well plates at 27°C in the presence of 5% CO_2.

Putative frataxin homologues 1 and 2 (NCBI Accession No. EAX980048 and EAY22979) from *T. vaginalis* strain G3 (= ATCC PRA-98) were PCR-amplified using oligonucleotides Tvftx1-F (5′-AAGCTTATGTTAAGCGGATTT TCT-3′) and Tvftx1-R (5′-GGATCCTTAGCAACCGAAAGCAGT-3′), and Tvftx2-F (5′-AAGCTTATGCTTAGTGGATTTTCA-3′) and Tvftx2-R (5′-GGATCCTTAACAACCAAATGCGGT-3′) respectively. PCR amplicons were cloned into pGEM T-Easy (Promega), liberated by digestion of insert-containing plasmid with HindIII and BamHI, and ligated into pABPURO (Rusconi *et al*., 2005) digested with the same enzymes, resulting in the constructs Tv-frataxin-1 and Tv-frataxin-2. These constructs as well as an empty pABPURO were separately electroporated into the clonal cell line 2 bearing Tb-Ftx-KD. After 2 weeks of cultivation, only cells resistant to 1 μg ml^{-1} puromycin survived, and these were cloned as described above.

To generate Tv-frataxin-2 fusion protein with HA3 tag, the tag was amplified from the pJH54 plasmid (kindly provided by Christine Clayton). The PCR product was digested with BamHI and EcoRI and ligated into the corresponding sites of pABPURO (Rusconi *et al*., 2005). Next, the Tv-frataxin-2 coding region lacking stop codon was inserted via HindIII and BamHI into the above-described construct, which was after linearization with BstXI introduced into the procyclic *T. brucei* strain 29-13. Cells resistant to 1 μg ml^{-1} puromycin were used for immunolocalization of Tv-frataxin-2.

Phylogenetic analysis

Available frataxin amino acid sequences were downloaded from the GenBank, and other publicly available databases (http://www.jgi.doe.gov/; http://www.jgi.doe.gov/). Sequences were aligned using CLUSTALX, gaps and unambiguously aligned regions were excluded from further analysis. The maximum likelihood tree (log lk = –6099.20593) was computed using PHYML program and the appropriate model for

amino acid substitutions was chosen by Prottest WAG (Abascal *et al.*, 2005). The tree was computed with discrete gamma distribution in four categories and all the parameters estimated form the data set (γ shape = 1.808 and proportion of invariants = 0.000). Numbers above branches indicate maximum-likelihood bootstrap support as computed from 300 replicates using the same model and settings.

Parasite cell culture

Procyclic *T. brucei* (cell line 29-13) was cultured at 27°C in SDM-79 medium (Vondrušková *et al.*, 2005). Bloodstream *T. brucei* (strain 920) was grown in rats and mice. Bloodstream trypanosomes were harvested from animals by cardiac exsanguination when the parasitaemia reached ~1×10^9 cell ml^{-1}. Blood was placed onto a DE52 DEAE cellulose (Whatman) column and washed with PSG buffer (38 mM Na_2HPO_4, 2 mM KH_2PO_4, 80 mM glucose, 29 mM NaCl, pH 8.0); eluted parasites were collected by centrifugation and the pellet was stored at –80°C until required.

Following Northern blot analysis, one clone from four Tb-frataxin RNAi cell lines was used for further experiments. Growth curves obtained over a period of 12 days following RNAi induction were established using the Beckman Z2 Cell Counter. Cell morphology was analysed under the light microscope and by staining with 4′,6-diamidino-2-phenylindole (DAPI).

Northern blotting

Approximately 5 μg of total RNA per lane was loaded on a 1% formaldehyde agarose gel, blotted and cross-linked as published elsewhere (Vondrušková *et al.*, 2005). After prehybridization in NaPi solution (0.25 M Na_2HPO_4 and 0.25 M NaH_2PO_4, pH 7.2, 1 mM EDTA, 7% SDS) for 2 h at 55°C, hybridization was performed overnight in the same solution at 55°C. A wash in 2× SSC + 0.1% SDS at room temperature for 20 min was followed by three washes in 0.2× SSC + 0.1% SDS for 20 min each at 55°C.

Preparation of antibodies and Western blotting

The entire coding region of *T. brucei* frataxin was PCR-amplified from genomic DNA, cloned into pRSET-A expression vector (Invitrogen), sequenced and propagated in *E. coli* strain BL21 Star DE3. Upon induction with 1 mM IPTG at 37°C, the cells were sonicated and the His-tagged overexpressed protein was purified from the supernatant using ProBond™ Ni^{2+}-chelating resin under native conditions as specified by the manufacturer (Invitrogen). Mass spectrometry analysis confirmed the identity of the protein (data not shown), which was used for the generation of specific polyclonal antibodies. Polyclonal antibodies in rabbits were prepared following a protocol described elsewhere (Vondrušková *et al.*, 2005). Cell lysates corresponding to 5×10^6 cells $lane^{-1}$ were separated on a 4–19% SDS-PAGE gradient gel. The polyclonal rabbit antibodies against *T. brucei* cytochrome *c*, TbIscU and TbIscS (Smíd *et al.*, 2006), aconitase (Saas *et al.*, 2000), hsp60 (Horváth *et al.*, 2005), and MRP2, TbMP81 and REAP1 (Vondrušková *et al.*, 2005), were used as described previously. Western blot bands were quantified with software Bio-Rad quantity one.

Digitonin fractionation and immunocytochemistry

Digitonin fractionation was performed following a protocol described previously (Smíd *et al.*, 2006). For mitotracker staining, cells were re-suspended in SDM-79 medium and incubated with 0.5 μM Mitotracker Red CMXRos (Molecular Probes) at 27°C for 10 min. Cells were then washed and incubated in fresh medium for an additional 20 min, and then washed twice with phosphate-buffered saline (PBS) buffer. Washed cell suspensions were spread on poly-L-lysine-coated slides and allowed to adhere for 30 min in a humid chamber at 27°C. Immunofluorescent localizations of Tb-frataxin and HA_3-tagged Tv-frataxin-2 were performed with slides fixed in ice-cold methanol for 5 min, followed by incubation in ice-cold acetone for an additional 5 min. The slides were pre-incubated at room temperature for 1 h with bovine serum albumin and gelatin (BSA+G) in PBS, followed by incubation with the mouse α-HA3 monoclonal antibody at 1:250 dilution in BSA+G in PBS for 1 h at room temperature. After washing three times for 5 min each in PBS on a rocking platform, the slides were incubated with secondary rabbit α-mouse antibody conjugated to Alexa Fluor 488 at a 1:1000 dilution, washed three times in PBS for 5 min each, and mounted in Vectashield containing DAPI. Cells were imaged using an Olympus IX81 microscope and images were captured using a Hamamatsu Orca-AG digital camera and cell^R imaging software. For the detection of Tb-frataxin, the rabbit polyclonal α-Tb-frataxin antibody was used at 1:200 dilutions, followed by secondary mouse α-rabbit antibody conjugated to Alexa Fluor 488.

In-gel digestion, mass spectrometry and sedimentation analysis

The Coomassie-stained band of putative overexpressed frataxin was cut from a SDS-PAGE gel, destained and subjected to cystein reduction and alkylation. After the alkylation the protein was in-gel digested with trypsin (Roche) at 37°C and the peptide mixture was applied onto a 180 μm capillary packed with 10 cm of RPC18 resin (Michrom Bioresources) and separated using a gradient elution. The column was attached to a nanoelectrospray ion source of the ion trap mass spectrometer (ThermoElectron). The MS/MS data were searched with Sequest software against NCBI non-redundant database. A total of 5×10^8 procyclic or 2×10^9 bloodstream-form cells were lysed and loaded on a 10–30% glycerol gradient as described previously (Vondrušková *et al.*, 2005).

Measurements of respiration rate, mitochondrial inner membrane potential and ROS

Exponentially growing cells (~5×10^6 cells ml^{-1}) were collected by centrifugation (800 *g*, 5 min, room temperature), washed, and re-suspended in 1 ml of fresh SDM-79 medium at a concentration of 3×10^7 cells ml^{-1}. Oxygen consumption

was determined with a Clark-type electrode (Strathkelvin Instruments), and total oxygen consumption over a 4 min time frame was determined. TMRE (Molecular Probes) uptake was used as a measure of the mitochondrial membrane potential as described previously (Horváth *et al.*, 2005). A total of 5×10^6 cells in the logarithmical growth were collected, washed, re-suspended in 1 ml of fresh SDM-79, and dihydroethidium (Sigma-Aldrich) was added to final concentration 5 μg ml^{-1} (Santos *et al.*, 2004). Cells were incubated at 27°C for 30 min, harvested and re-suspended in 5 ml of iso-flow. Intracellular free radicals were detected by an Epics XL flow cytometry (Beckman Coulter) with excitation and emission settings of 488 nm and 620 nm. Dihydroethidium can be oxidized by superoxide to fluorescent ethidium, which interacts with DNA (Carter *et al.*, 1994).

Enzyme assays and determination of metabolic end-products

Succinate dehydrogenase (complex II) activity was measured from 5 to 10 μg of soluble protein in mitochondria-rich fractions. Assay fractions were pre-incubated for 10 min at 30°C in plastic cuvettes containing 1 ml of the assay buffer (25 mM KH_2PO_4, pH 7.2; 5 mM $MgCl_2$; 20 mM sodium succinate). Next, rotenone (2 μg ml^{-1}), antimycin A (2 μg ml^{-1}), KCN (2 mM) and ubiquinone 2 (65 μM) were added and the specific activity of complex II was measured by following the reduction of 2.6-dichlorophenol-indophenol (DCIP; final concentration 50 μM) at 600 nm, assuming an extinction coefficient of 19.1 mM^{-1} cm^{-1}.

The activities of cytosolic and mitochondrial aconitase and mitochondrial threonine dehydrogenase were determined spectrophotometrically at 240 nm and 340 nm as production of *cis*-aconitate and rate of NAD^+ reduction respectively (Saas *et al.*, 2000). For fumarase measurements, cells were washed twice in ice-cold SHE buffer (250 mM glucose, 25 mM HEPES, pH 7.4; 1 mM EDTA), re-suspended in HBSS (Gibco) containing 0.1% Triton X-100 and incubated for 5 min on ice. After brief centrifugation (2000 *g*, 2 min), the activity of fumarase in the resulting supernatant was measured spectrophotometrically at 240 nm as the rate of production of fumarate. Mtabolic end-products were determined by HPLC as described previously (Smíd *et al.*, 2006).

Iron and zinc measurements

Samples digested with concentrated HNO_3 and subsequently treated with H_2O_2 were analysed by Inductively Coupled Plasma–Atomic Emission Spectroscopy (ICP-AES) using an Optima 3000 DV ICP Optical Emission Spectrometer (Perkin Elmer).

Acknowledgements

We thank De-Hua Lai, Miroslav Oborník and Jiří Týč for various contributions to this project. Michael Boshart, Christine Clayton, Paul A.M. Michels and Ken Stuart kindly provided antibodies or vectors. This work was supported by awards from the Grant Agency of the Czech Republic 204/06/1558, Grant Agency of the Czech Academy of Sciences A500960705, the Czech Ministry of Education (LC07032, 2B06129, 0021620858 and 6007665801) and the Royal Society. M.L.G. is a Royal Society University Research Fellow.

References

Abascal, F., Zardoya, R., and Posada, D. (2005) ProtTest: selection of best-fit models of protein evolution. *Bioinformatics* **21:** 2104–2105.

Bedekovics, T., Gajdos, G.B., Kispal, G., and Isaya, G. (2007) Partial conservation of functions between eukaryotic frataxin and the *Escherichia coli* frataxin homolog CyaY. *FEMS Yeast Res* **7:** 1276–1284.

Bencze, K.Z., Kondapalli, K.C., Cook, J.D., McMahon, S., Millan-Pacheco, C., Pastor, N., and Stemmler, T.L. (2006) The structure and function of frataxin. *Crit Rev Biochem Mol Biol* **41:** 269–291.

Besteiro, S., Barrett, M.P., Riviere, L., and Bringaud, F. (2005) Energy generation of insect stages of *Trypanosoma brucei*: metabolism in flux. *Trends Parasitol* **21:** 185–191.

Bochud-Allemann, N., and Schneider, A. (2002) Mitochondrial substrate level phosphorylation is essential for growth of procyclic *Trypanosoma brucei*. *J Biol Chem* **277:** 32849–32854.

Bulteau, A.-L., O'Neill, H.A., Kennedy, M.C., Ikeda-Saito, M., Isaya, G., and Szweda, L.I. (2004) Frataxin acts as an iron chaperone protein to modulate mitochondrial aconitase activity. *Science* **305:** 242–245.

Bulteau, A.-L., Dancis, A., Gareil, M., Gareil, M., Montagne, J.-J., Camadro, J.-M., and Lesuisse, E. (2007) Oxidative stress and protease dysfunction in the yeast model of *Friedreich ataxia*. *Free Rad Biol Med* **42:** 1561–1570.

Campanella, A., Isaya, G., O'Neill, H.A., Santambrogio, P., Cozzi, A., Arosio, P., and Levi, S. (2004) The expression of human mitochondrial ferritin rescues respiratory function in frataxin-deficient yeast. *Hum Mol Genet* **13:** 2279–2288.

Carlton, J.M., Hirt, R.P., Silva, J.C., Delcher, A.L., Schatz, M., Zhao, Q., *et al.* (2007) Draft genome sequence of the sexually transmitted pathogen *Trichomonas vaginalis*. *Science* **315:** 207–212.

Carter, W.O., Narayanan, P.K., and Robinson, J.P. (1994) Intracellular hydrogen peroxide and superoxide anion detection in endothelial cells. *J Leukoc Biol* **55:** 253–258.

Cavadini, P., Gellera, C., Patel, P.I., and Isaya, G. (2000) Human frataxin maintains mitochondrial iron homeostasis in *Saccharomyces cerevisiae*. *Hum Mol Genet* **9:** 2523–2530.

Cook, J.D., Bencze, K.Z., Jankovic, A.D., Crater, A.K., Busch, C.N., Bradley, P.B., *et al.* (2006) Monomeric yeast frataxin is an iron binding protein. *Biochemistry* **45:** 7767–7777.

Ding, H., Yang, J., Coleman, L.C., and Yeung, S. (2007) Distinct iron binding property of two putative iron donors for the iron–sulfur cluster assembly: IscA and the bacterial frataxin ortholog CyaY under physiological and oxidative stress conditions. *J Biol Chem* **282:** 7997–8004.

Dolezal, P., Dancis, A., Lesuisse, E., Sutak, R., Hrdy, I., Embley, T.M., and Tachezy, J. (2007) Frataxin, a con-

served mitochondrial protein, in the hydrogenosome of *Trichomonas vaginalis*. *Eukaryot Cell* **6:** 1431–1438.
van Dooren, G.G., Stimmler, L.M., and McFadden, G.I. (2006) Metabolic maps and functions of the *Plasmodium* mitochondrion. *FEMS Microbiol Rev* **30:** 596–630.
Embley, T.M. (2006) Multiple secondary origins of the anaerobic lifestyle in eukaryotes. *Philos Trans R Soc Lond B Biol Sci* **361:** 1055–1067.
Estévez, A.M., Haile, S., Steinbüchel, M., Quijada, L., and Clayton, C. (2004) Effects of depletion and overexpression of the *Trypanosoma brucei* ribonuclease L inhibitor homologue. *Mol Biochem Parasitol* **133:** 137–141.
Foury, F., and Talibi, D. (2001) Mitochondrial control of iron homeostasis. A genome wide analysis of gene expression in a yeast frataxin-deficient strain. *J Biol Chem* **276:** 7762–7768.
Gakh, O., Park, S., Liu, G., Macomber, L., Imlay, J.A., Ferreira, G.C., and Isaya, G. (2006) Mitochondrial iron detoxification is a primary function of frataxin that limits oxidative damage and preserves cell longevity. *Hum Mol Genet* **15:** 467–479.
Gerber, J., Mühlenhoff, U., and Lill, R. (2003) An interaction between frataxin and Isu1/Nfs1 that is crucial for Fe/S cluster synthesis on Isu1. *EMBO Rep* **4:** 906–911.
Gerber, J., Neumann, K., Prohl, C., Mühlenhoff, U., and Lill, R. (2004) The yeast scaffold proteins Isu1p and Isu2p are required inside mitochondria for maturation of cytosolic Fe/S proteins. *Mol Cell Biol* **24:** 4848–4857.
Ginger, M.L. (2006) Niche metabolism in parasitic protozoa. *Philos Trans R Soc Lond B Biol Sci* **361:** 101–118.
Gonzáles-Cabo, P., Vazquez-Manrique, R.P., García-Gimeno, M.A., Sanz, P., and Palau, F. (2005) Frataxin interacts functionally with mitochondrial electron transport chain proteins. *Hum Mol Genet* **14:** 2091–2098.
Hampl, V., Horner, D.S., Dyal, P., Kulda, J., Flegr, J., Foster, P.G., and Embley, T.M. (2005) Inference of the phylogenetic position of oxymonads based on nine genes: support for metamonada and excavata. *Mol Biol Evol* **22:** 2508–2518.
Hausler, T., Stierhof, Y.-D., Blattner, J., and Clayton, C. (1997) Conservation of mitochondrial targeting sequence function in mitochondrial and hydrogenosomal proteins from the early-branching eukaryotes *Crithidia, Trypanosoma* and *Trichomonas*. *Eur J Cell Biol* **73:** 240–251.
Horváth, A., Horáková, E., Dunajčíková, P., Verner, Z., Pravdová, E., Šlapetová, I., *et al.* (2005) Down-regulation of the nuclear-encoded subunits of the complexes III and IV disrupts their respective complexes but not complex I in procyclic *Trypanosoma brucei*. *Mol Microbiol* **58:** 116–130.
Irazusta, V., Cabiscol, E., Reverter-Branchat, G., Ros, J., and Tamarit, J. (2006) Manganese is the link between frataxin and iron–sulfur deficiency in the yeast model of *Friedreich ataxia*. *J Biol Chem* **281:** 12227–12232.
Jensen, L.T., and Culotta, V.C. (2000) Role of *Saccharomyces cerevisiae* ISA1 and ISA2 in iron homeostasis. *Mol Cell Biol* **20:** 3918–3927.
Johnson, D.C., Dean, D.R., Smith, A.D., and Johnson, M.K. (2005) Structure, function, and formation of biological iron–sulfur clusters. *Annu Rev Biochem* **74:** 247–281.
Kaut, A., Lange, H., Diekert, K., Kispal, G., and Lill, R. (2000) Isa1p is a component of the mitochondrial machinery for maturation of cellular iron–sulfur proteins and requires conserved cysteine residues for function. *J Biol Chem* **275:** 15955–15961.
Keeling, P.J., Burger, G., Durnford, D.G., Lang, B.F., Lee, R.W., Pearlman, R.E., *et al.* (2005) The tree of eukaryotes. *Trends Ecol Evol* **20:** 670–676.
Kispal, G., Sipos, K., Lange, H., Fekete, Z., Bedekovics, T., Janaky, T., *et al.* (2005) Biogenesis of cytosolic ribosomes requires the essential iron-sulphur protein Rli1p and mitochondria. *EMBO J* **24:** 589–598.
Lang, B.F., Burger, G., O'Kelly, C.J., Cedergren, R., Golding, G.B., Lemieux, C., *et al.* (1997) An ancestral mitochondrial DNA resembling a eubacterial genome in miniature. *Nature* **387:** 493–497.
Lesuisse, E., Santos, R., Matzanke, B.F., Knight, S.A., Camadro, J.M., and Dancis, A. (2003) Iron use for haeme synthesis is under control of the yeast frataxin homologue (Yfh1). *Hum Mol Genet* **12:** 879–889.
Li, D.S., Ohshima, K., Jiralerspong, S., Bojanowski, M.W., and Pandolfo, M. (1999) Knock-out of the *cyaY* gene in *Escherichia coli* does not affect cellular iron content and sensitivity to oxidants. *FEBS Lett* **456:** 13–16.
Lill, R., and Mühlenhoff, U. (2006) Iron–sulfur protein biogenesis in eukaryotes: components and mechanisms. *Annu Rev Cell Dev Biol* **22:** 457–486.
Loiseau, L., Gerez, C., Bekker, M., Ollagnier-de Choudens, S., Py, B., Sanakis, Y., *et al.* (2007) ErpA, an iron sulfur (Fe S) protein of the A-type essential for respiratory metabolism in *Escherichia coli*. *Proc Natl Acad Sci USA* **104:** 13626–13631.
Martelli, A., Wattenhofer-Donze, M., Schmucker, S., Bouvet, S., Reutenauer, L., and Puccio, H. (2007) Frataxin is essential for extramitochondrial Fe–S cluster proteins in mammalian tissues. *Hum Mol Genet* **16:** 2651–2658.
Morrison, H.G., McArthur, A.G., Gillin, F.D., Aley, S.B., Adam, R.D., Olsen, G.J., *et al.* (2007) Genomic minimalism in the early diverging intestinal parasite *Giardia lamblia*. *Science* **317:** 1921–1926.
Mühlenhoff, U., Richhardt, N., Ristow, M., Kispal, G., and Lill, R. (2002) The yeast frataxin homolog Yfh1p plays a specific role in the maturation of cellular Fe/S proteins. *Hum Mol Genet* **11:** 2025–2036.
Nachin, L., Loiseau, L., Expert, D., and Barras, F. (2003) SufC: an unorthodox cytoplasmic ABC/ATPase required for [Fe–S] biogenesis under oxidative stress. *EMBO J* **22:** 427–437.
O'Neill, H.A., Gakh, O., and Isaya, G. (2004) Supramolecular assemblies of human frataxin are formed via subunit–subunit interactions mediated by a non-conserved amino-terminal region. *J Mol Biol* **345:** 433–439.
Park, S., Gakh, O., O'Neill, H.A., Mangravita, A., Nichol, H., Ferreira, G., and Isaya, G. (2003) Yeast frataxin sequentially chaperones and stores iron by coupling protein assembly with iron oxidation. *J Biol Chem* **278:** 31340–31351.
Pelzer, W., Mühlenhoff, U., Diekert, K., Siegmund, K., Kispal, G., and Lill, R. (2000) Mitochondrial Isa2p plays a crucial role in the maturation of cellular iron–sulfur proteins. *FEBS Lett* **476:** 134–139.
Ramazzotti, A., Vanmansart, V., and Foury, F. (2004) Mitochondrial functional interactions between frataxin and

Isu1p, the iron–sulfur cluster scaffold protein, in *Saccharomyces cerevisiae*. *FEBS Lett* **557:** 215–220.
Rodríguez-Ezpeleta, N., Brinkmann, H., Burger, G., Roger, A., Gray, M., Philippe, H., and Lang, B. (2007) Toward resolving the eukaryotic tree: the phylogenetic positions of jakobids and cercozoans. *Curr Biol* **17:** 1420–1425.
Rusconi, F., Durand-Dubief, M., and Bastin, P. (2005) Functional complementation of RNA interference mutants in trypanosomes. *BMC Biotechnol* **5**: Art. No. 6.
Saas, J., Ziegelbauer, K., von Haeseler, A., Fast, B., and Boshart, M. (2000) A developmentally regulated aconitase related to iron-regulatory protein-1 is localized in the cytoplasm and in the mitochondrion of *Trypanosoma brucei*. *J Biol Chem* **275:** 2745–2755.
Santos, R., Buisson, N., Knight, S.A.B., Dancis, A., Camadro, J.-M., and Lesuisse, E. (2004) *Candida albicans* lacking the frataxin homologue: a relevant yeast model for studying the role of frataxin. *Mol Microbiol* **54:** 507–519.
Schneider, A., Bursac, D., and Lithgow, T. (2008) The direct route: a simplified pathway for protein import into the mitochondrion of trypanosomes. *Trends Cell Biol* **18:** 12–18.
Schoenfeld, R.A., Napoli, E., Wong, A., Zhan, S., Reutenauer, L., Morin, D., *et al.* (2005) Frataxin deficiency alters heme pathway transcripts and decreases mitochondrial heme metabolites in mammalian cells. *Hum Mol Genet* **14:** 3787–3799.
Scott, D.A., Docampo, R., Dvorak, J.A., Shi, S., and Leapman, R.D. (1997) In situ compositional analysis of acidocalcisomes in Trypanosoma cruzi. *J Biol Chem* **272:** 28020–28029.
Shan, Y., Napoli, E., and Cortopassi, G. (2007) Mitochondrial frataxin interacts with ISD11 of the NFS1/ISCU complex and multiple mitochondrial chaperones. *Hum Mol Genet* **16:** 929–941.
Simpson, A.G., Inagaki, Y., and Roger, A.J. (2005) Comprehensive multigene phylogenies of excavate protists reveal the evolutionary positions of 'primitive' eukaryotes. *Mol Biol Evol* **23:** 615–625.
Smíd, O., Horáková, E., Vilímová, V., Hrdý, I., Cammack, R., Horváth, A., *et al.* (2006) Knock-downs of mitochondrial iron–sulfur cluster assembly proteins IscS and IscU down-regulate the active mitochondrion of procyclic *Trypanosoma brucei*. *J Biol Chem* **281:** 28679–28686.
Stehling, O., Elsasser, H.P., Bruckel, B., Mühlenhoff, U., and Lill, R. (2004) Iron–sulfur protein maturation in human cells: evidence for a function of frataxin. *Hum Mol Genet* **13:** 3007–3015.
Takahashi, Y., and Tokumoto, U. (2002) A third bacterial system for the assembly of iron–sulfur clusters with homologs in archaea and plastids. *J Biol Chem* **277:** 28380–28383.
Tovar, J., Leon-Avila, G., Sanchez, L.B., Sutak, R., Tachezy, J., van der Giezen, M., *et al.* (2003) Mitochondrial remnant organelles of *Giardia* function in iron-sulphur protein maturation. *Nature* **426:** 172–176.
Vivas, E., Skovran, E., and Downs, D.M. (2006) Salmonella enterica strains lacking the frataxin homolog CyaY show defects in Fe–S cluster metabolism in vivo. *J Bacteriol* **188:** 1175–1179.
Vondrušková, E., van den Burg, J., Zíková, A., Ernst, N.L., Stuart, K., Benne, R., and Lukeš, J. (2005) RNA interference analyses suggest a transcript-specific regulatory role for MRP1 and MRP2 in RNA editing and other RNA processing in *Trypanosoma brucei*. *J Biol Chem* **280:** 2429–2438.
Wickstead, B., Ersfeld, K., and Gull, K. (2002) Targeting of a tetracycline-inducible expression system to the transcriptionally silent minichromosomes of *Trypanosoma brucei*. *Mol Biochem Parasitol* **125:** 211–216.
Yoon, T., and Cowan, J.A. (2003) Iron–sulfur cluster biosynthesis. Characterization of frataxin as an iron donor for assembly of [2Fe–2S] clusters in ISU-type proteins. *J Am Chem Soc* **125:** 6078–6084.
Yoon, T., and Cowan, J.A. (2004) Frataxin-mediated iron delivery to ferrochelatase in the final step of heme biosynthesis. *J Biol Chem* **279:** 25943–25946.
Zhang, Y., Lyver, E.R., Knight, S.A., Pain, D., Lesuisse, E., and Dancis, A. (2006) Mrs3p, Mrs4p, and frataxin provide iron for Fe–S cluster synthesis in mitochondria. *J Biol Chem* **281:** 22493–22502.

Supplementary material

This material is available as part of the online article from:
http://www.blackwell-synergy.com/doi/abs/10.1111/j.1365-2958.2008.06260.x
(This link will take you to the article abstract).

Please note: Blackwell Publishing is not responsible for the content or functionality of any supplementary materials supplied by the authors. Any queries (other than missing material) should be directed to the corresponding author for the article.

